Broadband photonic-assisted microwave receiver with high cross-channel interference suppression and image rejection

SHENGKANG ZENG,[1] JIEJUN ZHANG,[1,*] LINGZHI LI,[1] RUIQI ZHENG,[1] YIRAN GUAN,[1] JINGXU CHEN,[1] YU QIAO,[1] QIULIN ZHANG,[1] AND JIANPING YAO[1,2]

[1]*Guangdong Provincial Key Laboratory of Optical Fiber Sensing and Communications, Institute of Photonics Technology, Jinan University, Guangzhou 511443, China*
[2]*Microwave Photonics Research Laboratory, School of Electrical Engineering and Computer Science, University of Ottawa, Ottawa, ON K1N 6N5, Canada*
*zhangjiejun@jnu.edu.cn

Abstract: A broadband photonic-assisted microwave receiver with high cross-channel interference suppression and image rejection is proposed and experimentally demonstrated. At the input of the microwave receiver, a microwave signal is injected into an optoelectronic oscillator (OEO), which functions as a local oscillator (LO) to generate a low-phase noise LO signal as well as a photonic-assisted mixer to down-convert the input microwave signal to the intermediate frequency (IF). A microwave photonic filter (MPF), realized by the joint operation of a phase modulator (PM) in the OEO and a Fabry-Perot laser diode (FPLD), is used as a narrowband filter to select the IF signal. Thanks to the wide bandwidth of the photonic-assisted mixer and the wide frequency tunable range of the OEO, the microwave receiver can support broadband operation. The high cross-channel interference suppression and image rejection are enabled by the narrowband MPF. The system is evaluated experimentally. A broadband operation from 11.27 to 20.85 GHz is demonstrated. For a multi-channel microwave signal with a channel spacing of 2 GHz, a cross-channel interference suppression ratio of 21.95 dB and an image rejection ratio of 21.51 dB are realized. The spurious-free dynamic range (SFDR) of the receiver is also measured to be 98.25 dB·Hz$^{2/3}$. The performance of the microwave receiver for multi-channel communications is also experimentally evaluated.

1. Introduction

A microwave receiver is a key subsystem in a microwave system such as a radar and a wireless communications system [1]. The broadband operation of a microwave receiver can be realized by using a wide frequency tunable local oscillator (LO) to down-convert a received radio frequency (RF) signal at a broadband mixer to an intermediate frequency (IF). In a multi-channel microwave communications system, an electrical filter must be used in the receiver to select the desired signal for a specific channel while suppressing cross-channel interference [2,3]. In addition, a microwave receiver should also have the ability to reject the image which cannot be filtered out directly by an electrical filter, or the microwave receiver should have a balanced Hartley architecture through which the image components are fully eliminated [2,3]. To fulfill the need for modern microwave systems, a microwave receiver is required to have a large bandwidth and operate in high-frequency bands with high flexibility and reconfigurability [1,4,5]. However, the incorporation of electrical filters makes a microwave receiver costly and bulky, especially when large frequency tunability is needed while providing high cross-channel interference suppression and image rejection [2–6].

A solution to achieve a wide-frequency tunable microwave receiver with high cross-channel interference suppression and image rejection is to implement the mixer and filter using photonics [1,7]. Instead of using electrical nonlinearity, the frequency down-conversion at a photonic mixer can be realized based on optical or optoelectronic nonlinearity with a much wider bandwidth [1]. For example, all-optical nonlinearity can be achieved using optical components such as a semiconductor optical amplifier (SOA) [8] or a highly nonlinear optical fiber (HNLF) [9]. In [8], an optical carrier modulated by an RF signal is injected with a local oscillator (LO) signal into an SOA, thanks to the cross-gain modulation in the SOA, a frequency down-converted optical sideband is generated, which is converted to an electrical IF signal at a photodetector (PD). In [9], an optical carrier modulated by an RF signal and a two-tone optical signal are injected into an HNLF, and an electrical IF signal is generated at a PD by detecting the optical signals produced through four-wave mixing. Frequency down-conversion based on optoelectronic nonlinearity can be achieved based on direct or indirect optical modulation and photodetection. By modulating an LO and an RF signal on an optical carrier and detecting the modulated optical signal at a PD, a frequency down-converted signal is generated due to the square-law detection property of a PD [10–13].

To achieve high cross-channel interference suppression and image rejection, a high Q-factor microwave filter is needed. Photonic solutions to achieve high cross-channel interference suppression and image rejection have been reported. In addition to wide bandwidth, photonic solutions can also provide large tunability. In [14], a microwave photonic filter (MPF) was incorporated into a photonics-based microwave mixer. A down-converted IF signal is selected by the MPF with high cross-channel interference suppression and image rejection. The MPF was realized based on phase-modulation to intensity-modulation (PM-IM) conversion by passing one sideband through the gain or loss spectrum of stimulated Brillouin scattering (SBS). In [15], an MPF based on PM-IM conversion and on-chip SBS was incorporated into a photonics-based microwave mixer to realize image rejection with a simple structure. A photonics-based microwave mixer with a balanced Hartley architecture can inherently eliminate the image component without using an MPF [16–20]. Photonics-based microwave mixers with a balanced Hartley architecture based on cascaded modulators [16,17] or 90-degree optical hybrids [18–20] have been reported. But to fully reject the image component, the time delays of the two channels must be precisely balanced and stabilized. In addition, the approach does not support cross-channel interference suppression without the use of electrical filters. Thus, the use of an MPF would be a better solution for high image rejection in addition to the capability of cross-channel interference suppression.

For the photonic down-conversion techniques reported in [8–20], an external microwave source is needed to provide an LO signal, which can be realized using an electronic oscillator, but it has a small frequency tunable range and poor phase noise performance [21]. On the other hand, an optoelectronic oscillator (OEO) can generate a microwave signal with a much wider frequency tunable range and lower phase noise. An OEO has a hybrid optoelectronic system consisting of an electrical path and an optical path, with the two paths connected through a modulator and a PD. Since the optical path can be made long with a low loss, the Q-factor of the optoelectronic loop is large and the phase noise is low [22–29]. The use of an OEO to generate an LO signal for frequency down-conversion to improve the frequency tunable range of a microwave receiver has been reported [30,31]. To achieve frequency-tunable single-frequency oscillation, a frequency-tunable electrical bandpass filter is needed for mode selection [32]. However, it is difficult to implement a frequency-tunable electrical bandpass filter with a high Q-factor [33]. A solution is to implement the frequency-tunable bandpass filter based on photonics. For example, based on PM-IM conversion using a phase-shifted fiber Bragg grating (PS-FBG), a frequency-tunable bandpass filter was implemented [34].

By combining the two features of the wide frequency tunability of an OEO and the narrow bandwidth of an MPF, we have recently reported a photonic-assisted microwave receiver with a wide frequency tunable range and a high cross-channel interference suppression and image rejection [35]. In this paper, a more detailed study of the photonic-assisted microwave receiver is provided including a detailed mathematical analysis and comprehensive experimental investigation. In addition, the dynamic range of the microwave receiver in terms of spurious-free dynamic range (SFDR) is also studied. The ability of the microwave receiver for multi-channel communications is also experimentally evaluated.

2. Principle

The schematic of the proposed broadband photonic-assisted microwave receiver is shown in Fig. 1 with the optical spectra at the indicated locations of the system shown in Fig. 2. The receiver consists of an OEO module and an IF selection module (an MPF). The OEO module is used to generate an LO signal as well as act as a photonic-assisted mixer. The IF selection module is used to select the desired IF signal of a specific channel. Two laser diodes (LD1 and LD2) are used to generate two optical carriers with angular frequencies of ω_1 and ω_2, which are used as the optical carriers for the OEO module and the IF selection module.
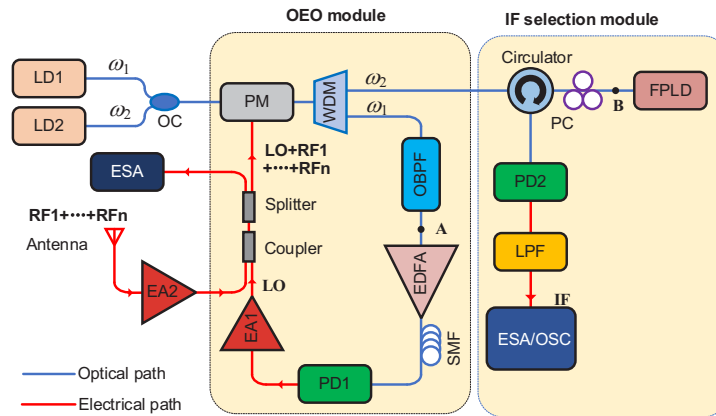
Fig. 1. Schematic of the proposed microwave receiver. LD: laser diode; OC: optical coupler; PM: phase modulator; WDM: wavelength division multiplexer; OBPF: optical bandpass filter; EDFA: erbium-doped fiber amplifier; SMF: single mode fiber; PD: photodetector; EA: electrical amplifier; PC: polarization controller; FPLD: Fabry-Perot laser diode; LPF: lowpass filter; ESA: electrical spectrum analyzer; OSC: oscilloscope.

In the OEO module, the optical carrier at ω_1 is modulated at the phase modulator (PM) and the optical signal at the output of the PM is sent to an optical bandpass filter (OBPF) followed by an erbium-doped fiber amplifier (EDFA). After amplification by the EDFA, the optical signal is sent to a photodetector (PD1) through a single-mode fiber (SMF), where an electrical signal is generated. The joint operation of the PM, the OBPF, and the PD1 forms an MPF (MPF1), which is used for oscillation frequency selection [36]. The signal at the output of PD1 is amplified by an electrical amplifier (EA1) and sent back to the PM via the RF port, to close an OEO loop. With a round-trip gain greater than the loss, the OEO can start to oscillate and an LO signal is generated [22].

Note that MPF1 is implemented based on phase modulation and PM-IM conversion, which is realized by removing one optical sideband by the OBPF to make the double sideband with carrier phase-modulated signal to be a single-sideband with carrier intensity-modulated signal. As shown in Fig. 2(a), the optical sideband at $\omega_1+\omega_{LO}$ is removed while the sideband at $\omega_1-\omega_{LO}$
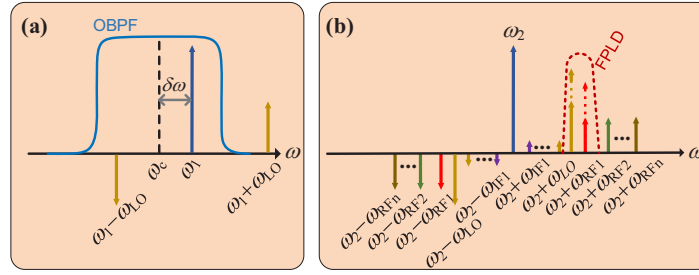
Fig. 2. (a) The optical spectrum of the phase-modulated optical signal and the frequency response of the OBPF at Point A in Fig. 1. By removing the optical sideband at $\omega_1+\omega_{\mathrm{LO}}$ with the help of the OBPF, the double sideband with carrier phase-modulated signal is converted to a single-sideband with carrier intensity-modulated signal. (b) The optical spectra of the optical carrier at ω_2 and its sidebands at Point B in Fig. 1. The sidebands at $\omega_2+\omega_{\mathrm{LO}}$ and $\omega_2+\omega_{\mathrm{RF1}}$ are selectively amplified by the FPLD to achieve PM-IM conversion. The red-dashed curve shows the gain spectrum at one mode of the FPLD.

and the optical carrier remain, which will beat with the optical carrier to generate an LO signal in PD1. If the OBPF has a central frequency of ω_c, MPF1 will be a bandpass filter with a central frequency that is the frequency difference between ω_c and ω_1, as illustrated in Fig. 2(a). By tuning the OBPF, the central frequency of MPF1 can be tuned.

For frequency down-conversion, the LO signal generated by the OEO is combined via an electrical coupler with a multi-channel RF signal (noted as RF1, RF2, ..., RFn) and applied to the PM, where the signals are modulated on the optical carriers at ω_1 and ω_2. The spectra of the optical carrier at ω_2 and its sidebands are shown in Fig. 2(b). After electro-optic modulation, multiple sidebands are generated around the optical carrier, including the +1st-order RF and LO sidebands, and the IF sidebands, which are terms generated due to the nonlinearity of the modulator, for example, the sideband at $\omega_2+\omega_{\mathrm{IF1}}$.

The optical carrier at ω_2 and its sidebands are then sent to the IF selection module through a wavelength division multiplexer (WDM). In the IF selection module, the optical signals are sent to the FPLD via an optical circulator for amplification. The optical signals reflected from the FPLD are sent to the PD2 via, again, the optical circulator, where an electrical signal is generated through photodetection. The joint operation of the PM, the FPLD, and the PD2 forms a secondary MPF (noted as MPF2) which is implemented based, again, on PM-IM conversion. But this time a Fabry-Perot laser diode (FPLD) is used to selectively amplify the sidebands at the desired frequencies at $\omega_2+\omega_{\mathrm{RF1}}$ and $\omega_2+\omega_{\mathrm{LO}}$, and all other sidebands and the optical carrier are reflected without amplification. As shown in Fig. 2(b), the sidebands at $\omega_2+\omega_{\mathrm{RF1}}$ and $\omega_2+\omega_{\mathrm{LO}}$ are selectively amplified after being reflected from the FPLD. The operation is equivalent to an MPF (MPF2) to select the IF signal at ω_{RF1}-ω_{LO}. The generated IF signal at the output of PD2 is applied to an electrical lowpass filter (LPF) to filter out undesired high-frequency components and sampled by an oscilloscope (OSC) for further processing.

In the following, a mathematical analysis is performed. First, we consider that only one RF signal and one LO signal are applied to the PM via the electrical coupler. The electric field of the optical carrier at ω_2 after being modulated at the PM is given by [37]

$$E_2(t) = E_{\mathrm{in2}}e^{j\omega_2 t} \sum_l \sum_m J_l(\beta_{\mathrm{RF}})J_m(\beta_{\mathrm{LO}})e^{j(l\cdot\omega_{\mathrm{RF}}+m\cdot\omega_{\mathrm{LO}})t} \tag{1}$$

where E_{in2} is the electric field of the optical carrier at ω_2, β_{RF} and β_{LO} are the modulation indices of the RF and LO signals applied to the PM, of which the angular frequencies are ω_{RF} and ω_{LO},

respectively, and l and m are the orders of the modulation sidebands by the RF and LO signals, J_l and J_m are the l-th and m-th order Bessel functions of the first kind, respectively.

Equation (1) shows that multiple optical sidebands are generated after the modulation as indicated in Fig. 2(b), of which the angular frequencies are determined by the orders of the Bessel functions and the RF and LO frequencies. After photodetection at a PD, we have a photocurrent, given by

$$
\begin{aligned}
I(t) &= R \cdot E_2(t) \cdot E_2(t)^* \\
&= RE_{in2}^2 \sum_l \sum_m \sum_p \sum_q J_l(\beta_{RF})J_m(\beta_{LO})J_p(\beta_{RF})J_q(\beta_{LO})e^{j[(l-p)\omega_{RF}+(m-q)\omega_{LO}]t}
\end{aligned}
\tag{2}
$$

where R is the responsivity of the PD. The photocurrent consists of multiple components that are generated due to the beating between two sidebands of different orders as well as the beating between the sidebands and the optical carrier at ω_2. To generate an IF signal, we let $|l\text{-}p|=1$ and $|m\text{-}q|=1$, in which the beating between the high-order sidebands is ignored due to their low amplitudes. Then, the IF component in the photocurrent can be expressed as

$$
\begin{aligned}
I_{IF}(t) &= 4RE_{in2}^2 J_0(\beta_{RF})J_0(\beta_{LO})J_1(\beta_{RF})J_1(\beta_{LO}) \cdot \cos(\omega_{IF}t) \\
&\quad + 4RE_{in2}^2 J_0(\beta_{RF})J_0(\beta_{LO}) \cdot J_1(\beta_{RF})J_1(\beta_{LO}) \cos(\omega_{IF}t + \pi)
\end{aligned}
\tag{3}
$$

The first term results from the beating between the $\pm$1st-order RF and LO sidebands, which are denoted as $\omega_2\pm\omega_{RF1}$ and $\omega_2\pm\omega_{LO}$ in Fig. 2(b). The second term results from the beating between the $\pm$1st-order IF sidebands and the optical carrier, which are denoted as $\omega_2\pm\omega_{IF1}$ and ω_2 in Fig. 2(b). They will fully cancel with each other because they are with equal amplitudes but opposite phases. Thus, the IF signal cannot be recovered. However, due to the PM-IM conversion using the FPLD by which the +1st order RF and LO sidebands are selectively amplified [38,39], an MPF (MPF2) is implemented to select the IF signal at $\omega_{RF}\text{-}\omega_{LO}$. The recovered IF signal can be expressed as

$$
I_{IF}(t) = 2RE_{in2}^2 \left(\sqrt{A_{RF}A_{LO}} - 1 \right) J_0(\beta_{RF})J_0(\beta_{LO})J_1(\beta_{RF})J_1(\beta_{LO}) \cos(\omega_{IF}t)
\tag{4}
$$

where A_{RF} and A_{LO} are the power gains of +1st-order RF and LO sidebands induced by the injection locking at the FPLD. Thanks to the narrow gain bandwidth of the FPLD, when multi-channel RF signals are applied to the PM together with the LO signal, only the optical sideband generated from the desired RF signal, e.g., RF1 and the LO signal which is tuned close to RF1 will be selectively amplified, as shown in Fig. 2(b), and an IF signal at $\omega_{RF1}\text{-}\omega_{LO}$ is generated.

Note that in addition to the capability of MPF2 for the desired IF signal selection, the narrow bandwidth of MPF2 enables high cross-channel interference suppression and image rejection when being employed in a microwave receiver.

3. Experiment and results

An experiment is performed based on the setup shown in Fig. 1. The two optical carriers at ω_1 and ω_2 are generated using a four-channel tunable laser source (Keysight N7714A). The PM (Photline MPZ-LN-40) in the OEO has a bandwidth of 40 GHz. The OBPF (Alnair Labs, BVF-300CL) has a tunable bandwidth of 3.7 to 370 GHz. The EDFA (PYOE PYOE-EDFA-C) has a maximum output power of 20 dBm. The SMF has a length of 80 m. PD1 (Finisar XYPD2120R) has a bandwidth of 50 GHz and a photoresponsivity of 0.65 A/W. The EAs (EA1 and EA2) (Realphoton RFA-4X25-EVB) have a bandwidth of 28 GHz, with a gain of 23 dB. An electrical spectrum analyzer (ESA) (Keysight N9020B) is used to monitor the signal generated by the OEO. A vector network analyzer (VNA) (Agilent N5222A) is used to measure the open-loop

frequency response of the OEO. The IF selection module shares the PM in the OEO module. The FPLD (Thorlabs FPL1009S) is used for selective amplification of the sidebands at the desired frequencies to achieve PM-IM conversion. PD2 (PIN/TIA20T) has a bandwidth of 20 GHz and a photoresponsivity of 0.6 A/W. The electrical LPF has a cutoff frequency of 6 GHz. An OSC (LabMaster 10 Zi-A) is used to sample the IF signal for further processing. The spectrum of the IF signal is measured by an ESA (Keysight N9020B). Two synthesized signal generators (Hittite HMC-T2220, HMC-T2240) are used to generate a multi-channel RF signal when measuring the spectrum of the IF signal, and an arbitrary waveform generator (Keysight M8194A) is used to generate a multi-channel communication signal when evaluating the operation of the microwave receiver for multi-channel communications.

3.1. Performance of the OEO module

The open-loop frequency response of the OEO is measured by the VNA and is shown in Fig. 3(a). As can be seen, the open-loop frequency response of the OEO is above 0 dB in a frequency range from 2.80 to 21.35 GHz, indicating that oscillation with a wideband frequency tunable range can be achieved. When the OEO loop is closed, an LO signal is generated. The measured spectra of a generated LO signal at different frequencies are shown in Fig. 3(b). As can be seen, the frequency of the generated LO signal is tuned from 4.94 to 20.30 GHz by tuning the central frequency of MPF1. Figure 3(c) shows a zoom-in view of the spectrum of a generated LO signal at 9.954 GHz in a frequency span of 10 MHz. The free spectral range (FSR) of the OEO loop is 2 MHz. The sidemode suppression ratio is up to 40.54 dB. The measured phase noise of the LO signal at 9.954 GHz is -100.19 dBc/Hz at a 10-kHz offset frequency, as shown in Fig. 3(d).
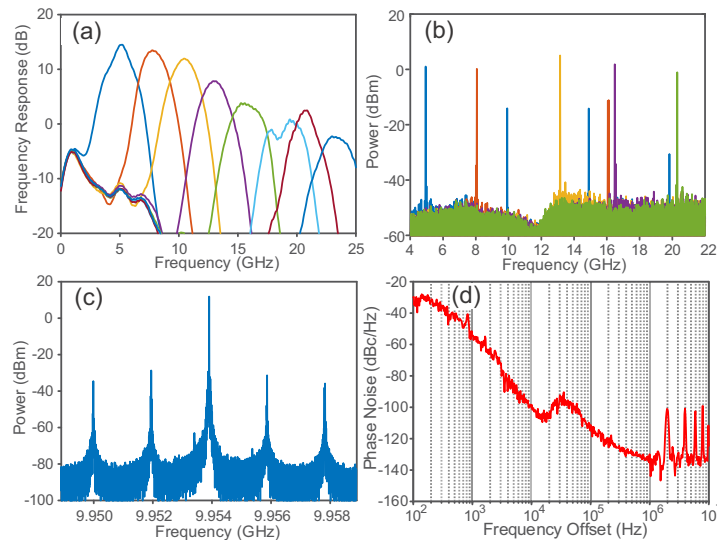

Fig. 3. (a) The open loop frequency response of the OEO when it is tuned, (b) the spectrum of the generated LO signal when the OEO is tuned, (c) a zoom-in view of the spectrum at 9.954 GHz, and (d) the phase noise of a generated LO signal at 9.954 GHz.

## 3.2. Evaluation of photonic frequency down-conversion

To evaluate photonic-assisted frequency down-conversion, two RF signals (RF1 and RF2) are applied to the PM. The optical signal at ω_2 at the output of the PM is sent to the FPLD, where injection locking is performed. Figure 4 shows the optical spectrum after injection locking. As can be seen, the +1st-order LO sideband at $\omega_2+\omega_{LO}$ and the RF1 sideband at $\omega_2+\omega_{RF1}$

are selectively amplified, while the other sidebands are reflected without amplification. The photodetection of the LO and the RF1 sidebands would generate an IF signal at ω_{RF1}-ω_{LO}.
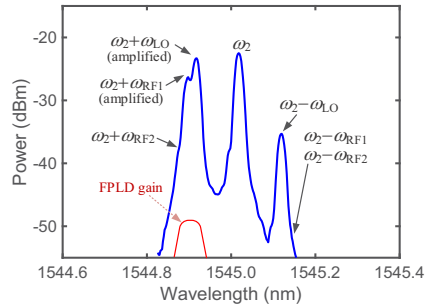
Fig. 4. Optical spectrum of the signal at the output of the FPLD centered at ω_2. Note that the sidebands at $\omega_2 + \omega_{\text{RF2}}$, ω_2-ω_{RF1}, and ω_2-ω_{RF2} are too weak to be observed in the measured spectrum due to the high-power level of the optical carrier and the LO sideband, and the absence of amplification from the FPLD.

In the experiment, the frequencies of the two RF signals are 17.52 and 19.38 GHz with an identical power of -20 dBm, which are generated by the two synthesized signal generators. The electrical spectrum of the signal at the output of PD2 is measured and is shown in Fig. 5(a). As can be seen, a strong IF signal (IF1) at 2.48 GHz is generated. A weak IF signal (IF2) due to the mixing between the LO and RF2 signal at 4.34 GHz is also seen, which is not fully eliminated by MPF2. Other frequency components including the second harmonic (SH) of IF1 (4.96 GHz) and the beat frequency signal (noted as difference frequency, DF) (1.86 GHz) between the two RF signals are also observed due to again the incomplete filtering by MPF2. The powers of IF1 and IF2 are -23.53 and -45.48 dBm, respectively. Although IF2 exists at the output of the microwave receiver, since it is over 20 dB smaller than IF1, it has little influence on the IF1 signal, showing a high cross-channel interference suppression.
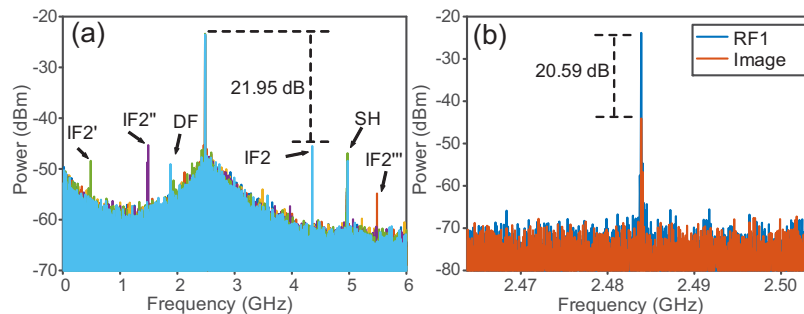

Fig. 5. (a) Spectra of the down-converted IF signals at the output of the microwave receiver. When the RF2 signal is tuned at four different frequencies, four IF signals (IF2, IF2′, IF2″, and IF2‴) at four different frequencies are generated, but the power is 20-dB lower than the power of the IF signal from the RF1 signal. (b) Spectra of the IF signal from the RF1 signal (blue) and from its image (red).

To further evaluate the high cross-channel interference suppression, we tune the frequency of the RF2 signal from 7.57 to 19.38 GHz while maintaining the frequency of the RF1 signal fixed at 17.52 GHz. The spectra of the IF signals are also shown in Fig. 5(a), from which we can see for the RF2 signal tuned at three different frequencies, three IF signals (IF2′, IF2″ and IF2‴) at three different frequencies are generated. Again, the powers of the three IF signals are

all much lower than the power of IF1. A suppression ratio of over 21.95 dB for the cross-channel interference is achieved within the operation bandwidth of the microwave receiver.

The ability of the proposed microwave receiver to reject the image is also evaluated, which is done by applying an image of the RF1 signal with a frequency of 12.55 GHz to the PM. Since the optical sidebands generated from the image are outside the amplification band of the FPLD (or equivalently its down-converted IF signal is outside the passband of MPF2), the IF signal from the image cannot be recovered, as indicated by Eq. (3). As shown in Fig. 5(b), the power of IF1 is 20.59 dB higher than that of the IF signal from the image, indicating strong image rejection capability of the microwave receiver.

The broadband operation of the microwave receiver is also evaluated, which is done by tuning the frequency of the RF1 signal from 11.27 to 20.85 GHz. To maintain a fixed IF frequency, the frequency of the LO signal is tuned accordingly. With such a large frequency tunable range, the microwave receiver can maintain a good performance. As can be seen, the variations of the cross-channel interference suppression ratio, image rejection ratio, and power of the IF signal are within 3.48 dB, 3.35 dB, and 0.79 dB, respectively, as shown in Fig. 6. The broadband operation of the microwave receiver is demonstrated.
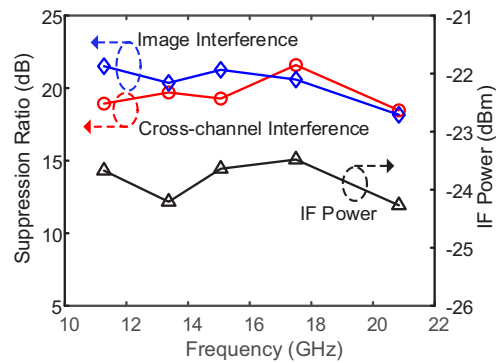
Fig. 6. The interference suppression ratio, image rejection ratio, and IF power when the frequency of the RF1 signal is tuned from 11.27 to 20.85 GHz.

The operating frequency range of the receiver is determined by the FSR of the FPLD and the cutoff frequency of the LPF. Due to the double sideband modulation of the PM, the frequencies of the received microwave signals should be less than half of the FSR of the FPLD, which is 44 GHz. Thus, the upper end of the operating frequency range is 22 GHz. Besides, the frequency of the LO signal is set to be higher than 8.5 GHz to avoid LO leakage. With a frequency spacing of 2.5 GHz between the LO and microwave signals, the frequency of the microwave signal should be higher than 11 GHz, i.e., the lower end will be about 11 GHz. It is believed that the operating frequency range can be extended by utilizing an FPLD with a larger FSR.

From Fig. 6, the mean power of the IF signal is -23.85 dBm. With the power of the input microwave signal of -20 dBm, the link gain is estimated to be -3.85 dB, indicating a high conversion efficiency between the RF and IF signals thanks to the high responsivity of the PD2 module with an integrated electrical amplifier, and the amplification of the +1st-order LO and RF1 sidebands brought by the FPLD.

The SFDR of the microwave receiver, a performance measure to evaluate the dynamic range of a microwave receiver, is also measured. The measurement is done based on a two-tone test in which a two-tone signal at 17.20 and 17.22 GHz is applied to the input of the proposed microwave receiver. By adjusting the power of the input signal from -26 to -18 dBm, the powers of the output IF signals and the third-order intermodulation distortion (IMD3) signals of the corresponding

input signals are measured. For a noise floor of -163.54 dBm/Hz, the SFDR is measured to be 98.25 dB·Hz$^{2/3}$, as shown in Fig. 7.
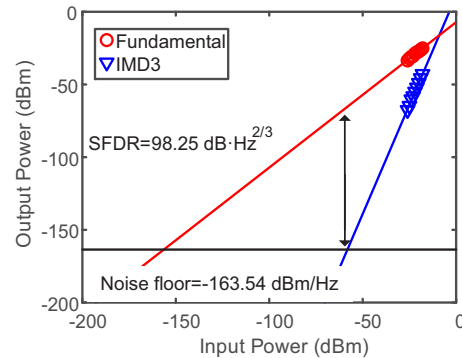

Fig. 7. SFDR measurement of the receiver. For a noise floor of -163.54 dBm/Hz, the SFDR is 98.25 dB·Hz$^{2/3}$.
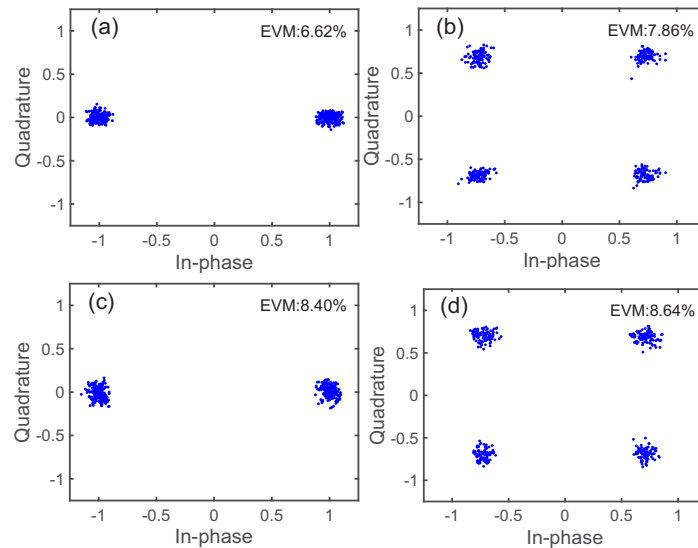
3.3. Evaluation of the microwave receiver for multi-channel communications

To evaluate the performance of the proposed receiver when being used for multi-channel communications, two experiments are performed. In the first experiment, only a single RF signal with two different modulation formats (Binary Phase Shift Keying, BPSK, and Quadrature Phase Shift Keying, QPSK) and two different symbol rates (500 MBaud, 1 GBaud) is applied to the PM. The frequency of the RF signal is tuned at 15.43 GHz, and the LO frequency is accordingly tuned at 12.93 GHz to make the IF frequency to be 2.5 GHz. The frequency down-converted IF signal is sampled by the OSC for further processing. A digital signal processing (DSP) algorithm is developed to track and compensate for the amplitude and phase drifts of the LO signal from the OEO [40,41]. For the RF signal with two different modulation formats (BPSK, QPSK) at a symbol rate of 500 MBaud, the constellation diagrams are shown in Fig. 8(a) and (b), respectively. The error vector magnitudes (EVMs) are measured to be 5.13% for the BPSK format and 5.53% for the QPSK format. When the symbol rate of the RF signal is increased from 500 MBaud to 1 GBaud, the EVMs are increased to 6.31% and 6.58% for the BPSK and QPSK formats, respectively. Clearly, the performance of the microwave receiver at a higher symbol rate is slightly reduced with the EVM increased from 5.53% for the 500 MBaud QPSK signal to 6.58% for the 1 GBaud QPSK signal. The noise figure of the receiver is estimated to be 15.3 dB by comparing the signal-to-noise ratios (SNRs) of the input and output signals.

In the second experiment, two RF signals at 13.69 and 20.36 GHz (RF1 and RF2) with modulation formats of BPSK and QPSK, respectively, are applied simultaneously to the PM. To switch between RF1 and RF2, the frequency of the LO signal is tuned between 11.19 and 17.86 GHz, to make the IF frequency at 2.5 GHz. When operating at 500 MBaud, the constellation diagrams are measured which are shown in Fig. 9(a) and (b), which are obtained with the assistance of the DSP algorithm. The EVMs are also calculated. As can be seen, the EVM for the RF2 signal with the QPSK format is 7.86%, which is slightly larger than that when only a single RF signal with the QPSK format is applied to the input of the microwave receiver (5.53%) due to the cross-channel interference. When operating at 1 GBaud, the constellation diagrams are also measured which are shown in Fig. 9(c) and (d), which are obtained again with the assistance of the DSP algorithm. The EVM is now 8.64%, which is again slightly higher than that when only a single RF signal with the same QPSK format is applied to the input of the microwave receiver (6.58%).
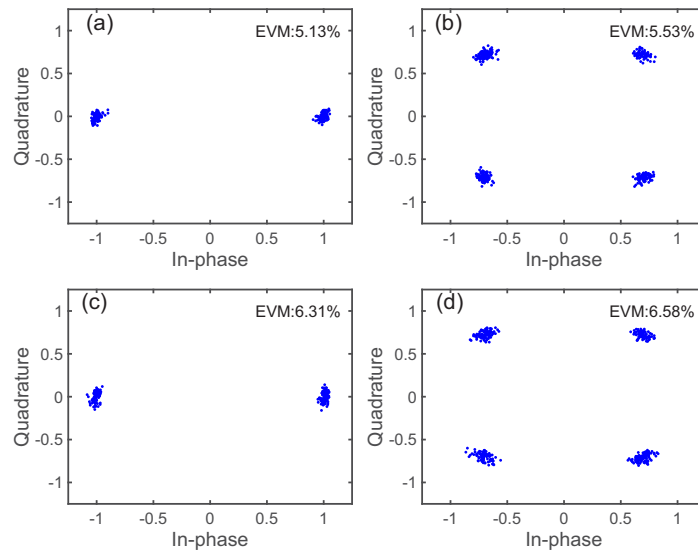
Fig. 8. Experimental results of using the microwave receiver when an RF signal with two different modulation formats at two different symbol rates is applied. Constellation diagrams for an RF signal at a symbol rate of 500 MBaud with the modulation formats of (a) BPSK and (b) QPSK. Constellation diagrams for an RF signal at a symbol rate of 1 GBaud with the modulation formats of (c) BPSK and (d) QPSK.

Fig. 9. Experimental results of using the microwave receiver for multi-channel communications. Constellation diagrams for two RF signals at a symbol rate of 500 MBaud with the modulation formats of (a) BPSK and (b) QPSK. Constellation diagrams for two RF signals at a symbol rate of 1 GBaud with the modulation formats of (c) BPSK and (d) QPSK.

4.   Conclusion

A broadband photonic-assisted microwave receiver with high cross-channel interference suppression and image rejection was proposed and demonstrated. A broadband tunable OEO was introduced as the LO signal generator to allow frequency tuning and channel switching of the microwave receiver for broadband operation. An MPF based on a PM-IM conversion using an FPLD was implemented to select the IF signal while suppressing the cross-channel interference and rejecting the image. Thanks to the wideband photonic-assisted mixing and the large frequency-tunable range offered by the OEO, wideband frequency down-conversion with high cross-channel interference suppression and image rejection was implemented. The proposed system was evaluated experimentally. The results showed cross-channel interference suppression ratio and image rejection ratio up to 21.95 and 21.51 dB were achieved, respectively. The performance of the microwave receiver when being used for multi-channel communications was also evaluated. The EVM performance was slightly increased by 2% when two RF signals were simultaneously applied to the input of the microwave receiver as compared with a single RF signal applied to the input, which was caused by the incomplete filtering of the other IF signal due to the mixing between the LO signal and the other RF signal.

In the experiments, a DSP algorithm was employed to track the amplitude and phase fluctuations of the LO signal from the OEO, which are caused due to the environmental changes to the long fiber in the OEO loop. The amplitude and phase fluctuations of the LO signal can be reduced if self-injection locking or a phase-locked loop is applied [42,43], which may further increase the system performance.

References

1. Z. Tang, Y. Li, J.P. Yao, and S. Pan, "Photonics-based microwave frequency mixing: Methodology and applications," Laser Photonics Rev. **14**(1), 1800350 (2020).
2. S. Mirabbasi and K. Martin, "Classical and modern receiver architectures," IEEE Commun. Mag. **38**(11), 132–139 (2000).
3. S. Bronckers, A. Roc'h, and B. Smolders, "Wireless receiver architectures towards 5G: Where are we?" IEEE Circuits Syst. Mag. **17**(3), 6–16 (2017).
4. G. Hueber, J. Tsutsumi, M. Seth, A. S. Morris, and R. B. Staszewski, "Cost-efficient high-volume transmission: Advanced transmission design and architecture of next generation RF modems and front-ends," IEEE Microwave **16**(7), 26–45 (2015).
5. S. Pan, D. Zhu, S. Liu, K. Xu, Y. Dai, T. Wang, J. Liu, N. Zhu, Y. Xue, and N. Liu, "Satellite payloads pay off," IEEE Microwave **16**(8), 61–73 (2015).
6. A. Liscidini, "Fundamentals of modern RF wireless receivers: A short tutorial," IEEE Solid State Circuits Mag. **7**(2), 39–48 (2015).
7. J. P. Yao, "Microwave photonics," J. Lightwave Technol. **27**(3), 314–335 (2009).
8. C. Bohémond, T. Rampone, and A. Sharaiha, "Performances of a photonic microwave mixer based on cross-gain modulation in a semiconductor optical amplifier," J. Lightwave Technol. **29**(16), 2404–2409 (2011).
9. Y. Gao, S. Gao, and H. Ou, "All-optical frequency converter based on fiber four-wave mixing for bidirectional radio-over-fiber systems," Microw. Opt. Technol. Lett. **51**(6), 1542–1545 (2009).
10. X. Fang, M. Bai, X. Ye, J. Miao, and Z. Zheng, "Ultra-broadband microwave frequency down-conversion based on optical frequency comb," Opt. Express **23**(13), 17111–17119 (2015).
11. V. R. Pagán, B. M. Haas, and T. E. Murphy, "Linearized electrooptic microwave downconversion using phase modulation and optical filtering," Opt. Express **19**(2), 883–895 (2011).
12. P. Li, W. Pan, X. Zou, S. Pan, B. Luo, and L. Yan, "High-efficiency photonic microwave downconversion with full-frequency-range coverage," IEEE Photonics J. **7**(4), 1–7 (2015).
13. C. Huang, E. Chan, and C. Albert, "Cascaded modulator topology for frequency conversion in antenna remoting applications," Appl. Opt. **58**(9), 2328–2333 (2019).

14. X. Kong, Y. Yu, H. Tang, and X. Zhang, "Microwave photonic image-reject mixer based on a tunable microwave photonic filter with high rejection," IEEE Photonics J. **10**(6), 1–11 (2018).

15. Z. Zhu, D. Choi, S. Madden, B. Eggleton, and M. Merklein, "High-conversion-gain and deep-image-rejection Brillouin chip-based photonic RF mixer," Opt. Lett. **45**(19), 5571–5574 (2020).

16. D. Shan, A. Wen, W. Zhai, X. Li, W. Zhang, and Z. Tu, "Filter-free image-reject microwave photonic downconverter based on cascaded modulators," Appl. Opt. **58**(13), 3432–3437 (2019).

17. P. Li, W. Pan, X. Zou, B. Lu, L. Yan, and B. Luo, "Image-free microwave photonic down-conversion approach for fiber-optic antenna remoting," IEEE J. Quantum Electron **53**(4), 1–8 (2017).

18. Z. Tang, D. Zhu, and S. Pan, "Coherent optical RF channelizer with large instantaneous bandwidth and large in-band interference suppression," J. Lightwave Technol. **36**(19), 4219–4226 (2018).

19. Y. Zhang, Z. Li, W. Chen, C. Liu, K. Shao, D. Zhu, and S. Pan, "Broadband image-reject mixing based on a polarization-modulated dual-channel photonic microwave phase shifter," IEEE Photonics J. **12**(2), 7800409 (2020).

20. W. Chen, D. Zhu, C. Xie, J. Liu, and S. Pan, "Microwave channelizer based on a photonic dual-output image-reject mixer," Opt. Lett. **44**(16), 4052–4055 (2019).

21. D. Zhu, S. Pan, S. Cai, and D. Ben, "High-performance photonic microwave downconverter based on a frequency-doubling optoelectronic oscillator," J. Lightwave Technol. **30**(18), 3036–3042 (2012).

22. X. S. Yao and L. Maleki, "Optoelectronic microwave oscillator," J. Opt. Soc. Am. B **13**(8), 1725–1735 (1996).

23. F. Zou, "Optoelectronic oscillator for 5 G wireless networks and beyond," J. Phys. D: Appl. Phys. **54**(42), 423002 (2021).

24. M. Li, L. Li, R. Cao, J. Zhang, and J. Yao, "Optoelectronic oscillator with improved sidemode suppression by joint use of spectral Vernier effect and parity-time symmetry," Opt. Express **30**(16), 28774–28782 (2022).

25. J. Fan, L. Li, J. Zhang, X. Feng, B. O. Guan, and J. P. Yao, "A parity-time-symmetric optoelectronic oscillator based on non-reciprocal electro-optic modulation," J. Lightwave Technol. **39**(8), 2305–2310 (2021).

26. J. Zhang and J. Yao, "Parity-time–symmetric optoelectronic oscillator," Sci. Adv. **4**(6), eaar6782 (2018).

27. T. Hao, Q. Cen, Y. Dai, J. Tang, W. Li, J.P. Yao, N. Zhu, and M. Li, "Breaking the limitation of mode building time in an optoelectronic oscillator," Nat. Commun. **9**(1), 1839 (2018).

28. T. Hao, Q. Cen, S. Guan, W. Li, Y. Dai, N. Zhu, and M. Li, "Optoelectronic parametric oscillator," Light: Sci. Appl. **9**(1), 102 (2020).

29. T. Hao, J. Tang, D. Domenech, W. Li, N. Zhu, J. Capmany, and M. Li, "Toward monolithic integration of OEOs: from systems to chips," J. Lightwave Technol. **36**(19), 4565–4582 (2018).

30. Z. Tang, F. Zhang, and S. Pan, "Photonic microwave downconverter based on an optoelectronic oscillator using a single dual-drive Mach-Zehnder modulator," Opt. Express **22**(1), 305–310 (2014).

31. F. Yang, D. Wang, Y. Wang, Z. Chen, T. Zhou, D. Yang, X. Zhong, and H. Zhang, "Photonics-assisted frequency up/down conversion with tunable OEO and phase shift," J. Lightwave Technol. **38**(23), 6446–6457 (2020).

32. X. Xie, C. Zhang, T. Sun, P. Guo, X. Zhu, L. Zhu, W. Hu, and Z. Chen, "Wideband tunable optoelectronic oscillator based on a phase modulator and a tunable optical filter," Opt. Lett. **38**(5), 655–657 (2013).

33. S. Pan and J. P. Yao, "Wideband and frequency-tunable microwave generation using an optoelectronic oscillator incorporating a Fabry–Perot laser diode with external optical injection," Opt. Lett. **35**(11), 1911–1913 (2010).

34. Y. Shao, X. Han, M. Li, Q. Liu, and M. Zhao, "Microwave downconversion by a tunable optoelectronic oscillator based on PS-FBG and polarization-multiplexed dual loop," IEEE Trans. Microw. Theory Techn. **67**(5), 2095–2102 (2019).

35. S. Zeng, J. Zhang, and J. P. Yao, "Photonic-Assisted Broadband Microwave Receiver with Cross-Channel Interference Suppression," *14th Int. Conf. Adv. Infocomm Technol.* 273–277 (IEEE, 2022).

36. T. Chen, X. Yi, L. Li, and R. Minasian, "Single passband microwave photonic filter with wideband tunability and adjustable bandwidth," Opt. Lett. **37**(22), 4699–4701 (2012).

37. V. R. Pagán and T. E. Murphy, "Electro-optic millimeter-wave harmonic downconversion and vector demodulation using cascaded phase modulation and optical filtering," Opt. Lett. **40**(11), 2481–2484 (2015).

38. W. Wang, L. Huang, J. Tao, H. Zhu, X. Du, L. Hao, C. Yu, and X. Chen, "Tunable multiple-passband microwave photonic filter based on external optical injected Fabry-Pérot laser," Opt. Express **27**(9), 12491–12503 (2019).

39. H. Chen, M. Lee, Y. H. Won, B. Nakarmi, and S. Pan, "High-Speed Switchable Dual-Passband Microwave Photonic Filter With Dual-Beam Injection in an SMFP-LD," J. Lightwave Technol. **39**(24), 7966–7972 (2021).

40. E. Ip and J. Kahn, "Feedforward carrier recovery for coherent optical communications," J. Lightwave Technol. **25**(9), 2675–2692 (2007).

41. D.-S. Ly-Gagnon, K. Katoh, and K. Kikuchi, "Unrepeatered optical transmission of 20 Gbit/s quadrature phase-shift keying signals over 210 km using homodyne phase-diversity receiver and digital signal processing," Electron. Lett. **41**(4), 59–60 (2005).

42. X. S. Yao and L. Maleki, "Opto-electronic oscillator for photonic systems," IEEE J. Quantum Electron. **32**(7), 1141–1149 (1996).

43. A. Banerjee, J. Sarkar, N. Das, and B. Biswas, "Phase-locking dynamics in optoelectronic oscillator," Opt. Commun. **414**, 119–127 (2018).